Cavity assisted high-resolution THz spectrometer

Fabien Simon, Coralie Elmaleh, Jean Decker, Marc Fourmentin, A. Cuisset, Guillaume Ducournau, Jean-Francois Lampin, Gaël Mouret, Francis Hindle

Photonics and Nanostructures - Fundamentals and Applications 58 (2024) 101227

Contents lists available at ScienceDirect

Photonics and Nanostructures - Fundamentals and Applications

journal homepage: www.elsevier.com/locate/photonics

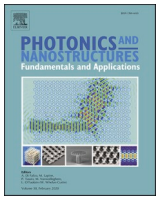

Cavity assisted high-resolution THz spectrometer

Fabien Simon [a], Coralie Elmaleh [a], Jean Decker [a], Marc Fourmentin [a], Arnaud Cuisset [a], Guillaume Ducournau [b], Jean-François Lampin [b], Gaël Mouret [a], Francis Hindle [a,*]

[a] Laboratoire de Physico-Chimie de l'Atmosphère, UR 4493, LPCA, Université du Littoral Côte d'Opale, Dunkerque, F-59140, France
[b] Institut d'Electronique, de Microélectronique et de Nanotechnologie, UMR CNRS 8520 Avenue Poincaré, B.P. 60069, Villeneuve d'Ascq, 59652, France

ARTICLE INFO

Keywords:
Terahertz spectroscopy
Cavity enhanced absorption spectroscopy
Cavity ring-down spectroscopy
Trace gas detection
Atmospheric propagation losses

ABSTRACT

The analysis of gases by THz radiation offers a high degree of discrimination due to the narrow linewidths that are observed at low pressure. The sensitivity of existing high-resolution instruments is limited by the availability and performance of critical system components. This study uses two key components with physical structures at the wavelength scale to realise a high finesse THz cavity. The cavity is characterised and incorporated into a spectrometer. Sensitivity limits of the instrument are experimentally demonstrated for trace and pure gases. Both CEAS (Cavity Enhanced Absorption Spectroscopy) and CRDS (Cavity Ring-Down Spectroscopy) configurations are shown to give sub-ppm detection levels. The cavity has also been used to measure the atmospheric losses.

1. Introduction

THz waves are often cited to have great potential for various applications such as, medical [1,2] and security imaging [3], non-destructive testing [4], high-speed communications [5,6], food freshness assessment [7] which have been demonstrated. The availability of high-performance system components for this wavelength region is critical to continue the development of these applications. THz spectroscopy has been perused using the technological building blocks available to the laboratories in question. High-resolution THz spectroscopy of gases has been successfully exploited by the astronomy community for many years [8]. Several airborne and land based instruments have already been deployed and require accurate and good quality laboratory data to interpret the measurements obtained, Herschel (0.4–8 THz) [9], GREAT SOFIA (1.25–2.5 THz) [10], ALMA (84–950 GHz) [11], Aura/MLS (240–640 GHz) [12] and TALIS (118–643 GHz) [13]. On the application side, the interest of using high-resolution THz spectroscopy is that it can provide an excellent molecular discrimination. At low pressure the observed molecular transitions are particularly narrow at room temperature only being limited by the Doppler broadening in the order of 1 MHz. Increasing the available sensitivity of such spectrometers is key to providing accurate spectroscopic data of a wide range of molecules for the interpretation of satellite data, and to enable gas analysis by THz at relevant concentration levels for applications like pollution detection and atmospheric monitoring. Infrared spectroscopy has already demonstrated instruments with very high sensitivity levels [14]. This performance was possible not only due to the use of powerful laser sources, but also the availability of high reflectivity spherical mirrors is essential. Indeed, the approach followed was to perform the spectroscopy inside a high finesse optical cavity. The light trapped in the cavity, with a weakly absorbing molecular species, makes many round trips. The effective interaction length between the light and the gas can reach many kilometres for a cavity that is no longer than 1 m. We have constructed a high finesse THz cavity whose components are tailored to the targeted wavelength. The cavity is incorporated into a spectrometer that can not only be used for a high-resolution spectroscopy, but also for the measurement of propagation losses of gaseous atmospheres.

2. THz cavity

Cavities employed in the infrared domain are typically composed of two high reflectivity spherical mirrors that are also the input and output couplers. The refocusing of the highly directional laser light is sufficient to avoid propagation losses and achieve excellent values of finesse. The construction of a THz cavity presents different challenges. An Amplified Multiplier Chain (AMC) is a convenient reliable monochromatic source that is commercially available for this frequency band. The radiation is generated in a rectangular waveguide and once launched into free space diverges much more strongly compared to an infrared laser. Secondly high reflectivity spherical mirrors are not commercially available for

* Corresponding author.
E-mail address: francis.hindle@univ-littoral.fr (F. Hindle).

https://doi.org/10.1016/j.photonics.2024.101227
Received 16 October 2023; Received in revised form 15 January 2024; Accepted 16 January 2024
Available online 20 January 2024

THz wavelengths. To overcome these obstacles, we choose to form a cavity using a THz waveguide closed by a pair of plane mirrors. The use of components with wavelength scale structuring has proven to be critical for the realisation of a high finesse THz cavity. In order to minimise the cavity losses an oversized corrugated waveguide was selected. Such circular waveguides [15–17] developed for the transmission of high power millimetre waves, have radii larger than the wavelength, and are structured with corrugations of λ/4 in depth. An electroformed waveguide, 20.54 mm in diameter and 48 cm long was fabricated by Thomas Keating Company. Designed for use at 600 GHz the corrugation depth was 125 μm by 83 μm wide having a pitch of 166 μm. The propagation losses of this waveguide have been estimated to be 0.004 dB/m [18].

Homemade photonic mirrors were constructed using a Bragg configuration. The transmission and reflectivity characteristics are dependent on the refractive index contrast, the layer thicknesses, and the number of periods. Such mirrors have already been demonstrated to provide an estimated reflectivity of 99.7 % [19]. The mirrors were formed using polished high resistivity silicon wafers of 25 mm in diameter. Spacers with a clear internal diameter of 21 mm are sandwiched between the discs to form the desired structure. Wafers with a thickness of 185+/–5 μm and spacers 375 +/–5 μm were assembled to target 600 GHz. Mirrors containing up to 6 periods have been investigated for this application. A matrix transfer calculation was used to predict the reflection band, for these dimensions indicating 550–650 GHz [20]. The maximum estimated reflectivity was calculated using an absorption of 0.02 cm^{-1} for the silicon wafers having a resistivity greater than 8 kΩ.cm, Table 1. The transmission of the mirrors was measured using a vector network analyser (VNA), Fig. 1. The forbidden band is observed to be centred around 609 GHz, whereas the calculation is centred at 600 GHz. The difference between the measured and calculated transmission spectra is attributed to the manufacturing tolerances of the wafers and spacers thicknesses. The available source power, waveguide and mirror losses and must be considered in order to select the most appropriate mirrors for the THz cavity. For example, this cavity with 3 period mirrors would have losses limited by the mirrors, yielding a finesse, F = 1000, and a transmission of T = 60 % at resonance. Conversely, if 5 period mirrors are used the waveguide losses are the limiting factor, giving F = 4300 and T = 1 %. The waveguide and mirror losses are similar when the 4 period mirrors are considered leading to a calculated performance of F= 3000 and T = 20 %. This solution is the optimal compromise between, a high finesse for long interaction lengths, and a sufficient signal level at the cavity output. As can be seen in the latter sections, finesse values greater than those predicted here may be observed. This is attributed to a small overestimation of either the silicon or waveguide losses. Nevertheless, this brief analysis enables the most suitable mirror configuration to be identified.

In order to eliminate the atmospheric absorption, the complete cavity was constructed and assembled inside a vacuum chamber with PTFE windows. An AMC (SGX, Virginia Diodes) covering the band from 500 to 750 GHz was used to characterise the cavity. This source can typically provide –21 dBm prior to the horn used to launch the radiation into free space. The AMC is fed by a standard microwave generator that can be operated in amplitude or frequency modulation (AM, FM). The source is coupled to the waveguided cavity, via the photonic mirror operating in transmission, using a TPX lens with a focal distance of 50 mm [21]. The lowest order hybrid electric modes HE_{11} is excited and presents the lowest losses. The second photonic mirror is also employed as an output coupler allowing the radiation transmitted by the cavity to be focused by a TPX lens with a focal distance of 50 mm, and measured using a Zero Biased Detector. Fig. 2.

Table 1
Calculated reflectivity and transmission of the silicon wafer photonic mirror structures around 600 GHz.

Periods	Reflectivity %	Transmission %
2	97.09	2.89
3	99.72	0.25
4	99.955	0.021
5	99.975	0.0018
6	99.977	0.00016

The source is operated in AM mode and a lock-in amplifier used to extract the amplitude of the modulated signal observed by the detector. In this way transmitted intensity can be measured while the source frequency steps over the target range point-by-point. A small section of the available frequency band is shown in Fig. 3.

Only two well defined cavity modes can be observed and are separated by 303.89 MHz. This is the Free Spectral Range (FSR) of the cavity corresponding to a distance of 49.3 cm. It is slightly longer than the physical dimension of the waveguide due to a small gap between the waveguide and each of the mirrors. Fitting the measured mode profiles with a Lorentzian function yielded values of the FWHM around 70 kHz, hence achievable values of Finesse (F) slightly in excess of 4000 (quality factor ≈ 8.9 $\times 10^6$). The variation of the finesse observed for successive cavity modes is attributed to the coupling of the high-finesse cavity with unwanted low-finesse cavities formed by the lenses, windows and horn antennae. If a weakly absorbing gas is injected into the cavity the effective path length for the interaction of the THz beam and the gas can be expected to be $2LF/\pi = 1.2km$, where L is the length of a single passage [22].

3. High-resolution spectrometer

The most straight-forward approach to harness the long interaction length of the cavity, for sensitive spectroscopy, would be to directly sample the target absorption spectrum with the successive cavity modes. This would provide only a single data point per cavity resonance, limiting the useful resolution to the FSR of the cavity. This may be overcome by having a fine control of the cavity length; indeed, a variation of λ/2 will allow a cavity mode to be positioned at any given frequency. In our case this is achieved using piezo-mechanical actuators to move on the mirrors by up to 300 μm. In order to simultaneously scan the AMC frequency and the frequency position of cavity a control loop was implemented. The cavity length was locked to the AMC frequency by applying a frequency modulation (FM). The profile of a cavity mode when measured in FM with a detection at the modulation frequency has a zero-crossing at the centre. This signal is used to feed a PID regulator that adjusts the cavity length, Fig. 4. A robust and reliable lock is easily achieved and maintained while sweeping the AMC frequency.

4. Results and discussion

4.1. Cavity Enhanced Absorption Spectroscopy (CEAS)

The use of a FM which is demodulated by a lock-in amplifier also provides the possibility to detect the harmonic at twice the modulation frequency. This signal has a non-zero value at the centre of the cavity mode. Its profile represents the second derivative of the AM mode profile. It is therefore not only sensitive to the peak transmitted intensity but also the mode width or finesse. This sensitive signal can be used to detect the presence of a weakly absorbing gas in the cavity. As this approach is based on the absorption it is known as CEAS, two examples are shown in Fig. 5 for trace gases. Calibrated trace gases purchased from Messer were used and contained either a single or multiple target species diluted in nitrogen, details in Table 2.

The left-hand pane of Fig. 5 shows the $J = 5 \leftarrow 4$ transition of CO for a concentration of 73.2 ppm. This molecule has a line strength of 3.28×10^{-22} $cm^{-1}/(molecule.cm^{-2})$ for a pure gas [23], hence for this trace gas with a concentration of 73.2 ppm the effective value is 2.4×10^{-26} $cm^{-1}/(molecule.cm^{-2})$. The measured baseline is displayed for this spectrum and demonstrates the stability of the instrument during

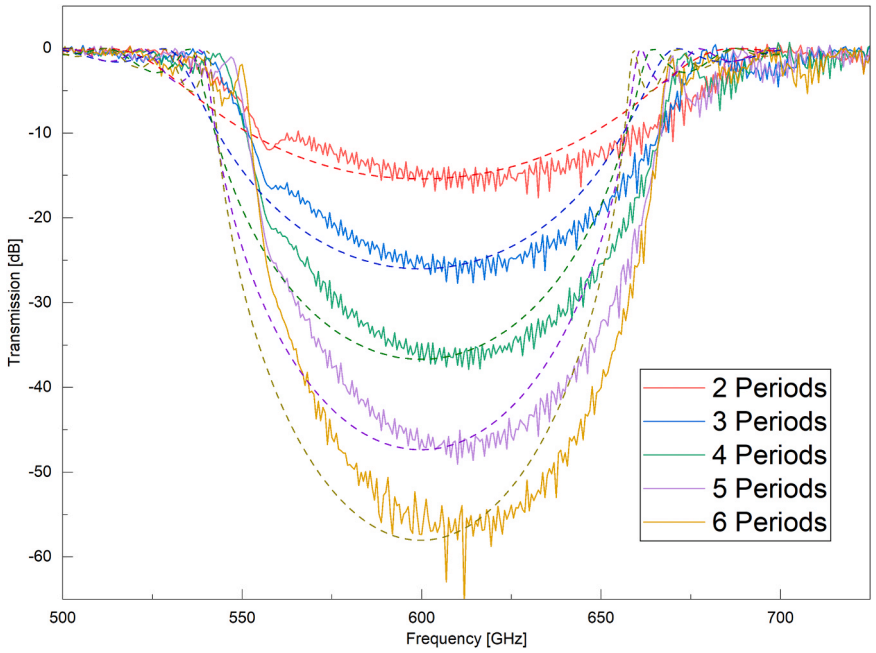

Fig. 1. Solid lines, Transmission measurements of the mirrors measured using a VNA, performed using Virginia Diodes WR1.5 500–750 GHz extension modules driven by a Rohde & Schwarz ZVA24. Calibration using a waveguided Through-Reflect-Match technique. Dashed lines, transmission calculated by matrix transfer method.

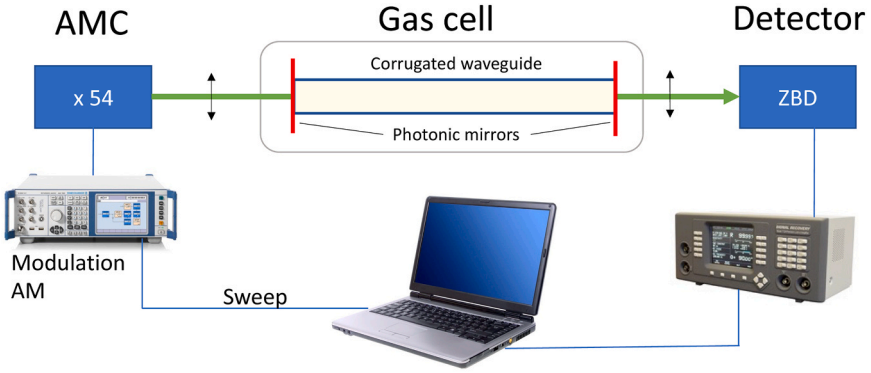

Fig. 2. Amplitude modulation characterisation of the cavity.

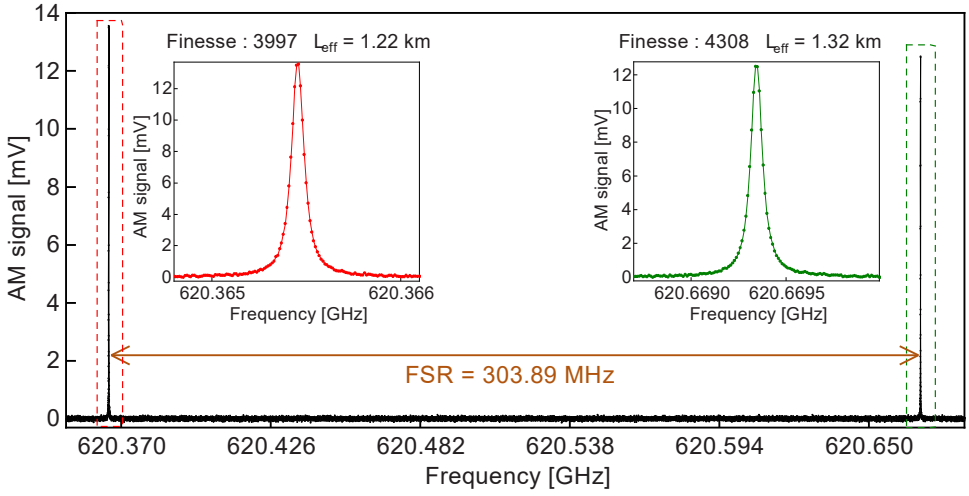

Fig. 3. Detected signal intensity transmitted by the cavity as a function of frequency covering slightly more than one free spectral range.

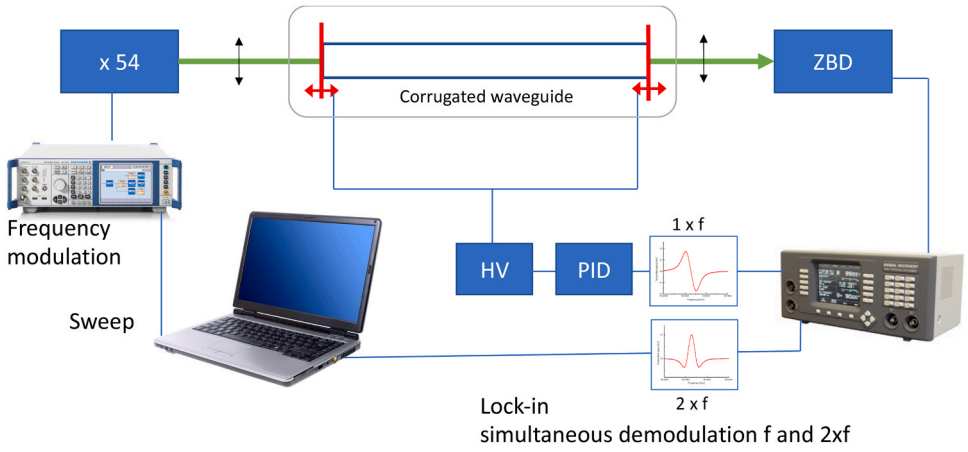

Fig. 4. Cavity assisted THz spectrometer in CEAS mode. The signal detected at the fundamental modulation frequency is used to lock the cavity to the source frequency. The second harmonic is sensitive to the amplitude and finesse of the cavity mode. Photonic mirrors placed on piezo-mechanical actuators.

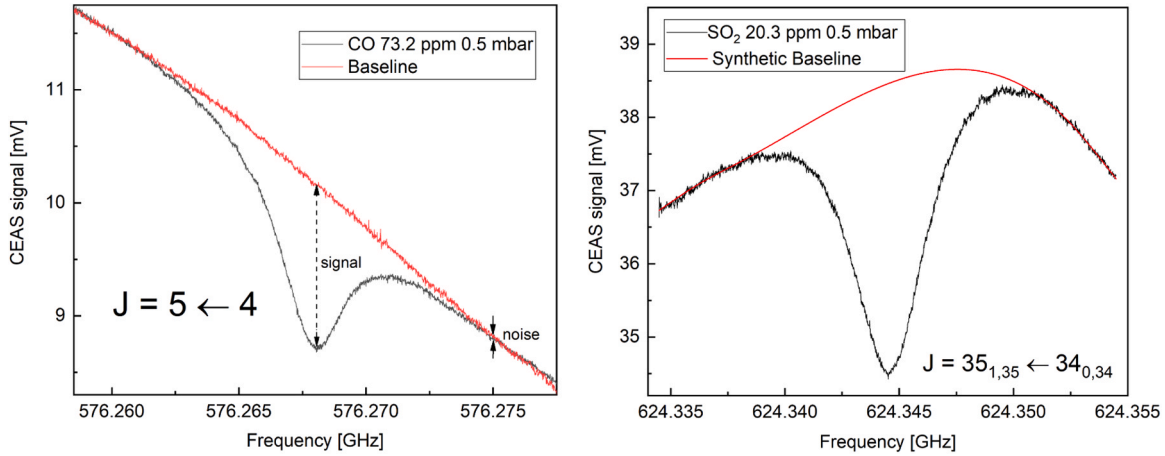

Fig. 5. Typical CEAS spectra covering approximately 20 MHz with a step size of 10 KHz. Left, a calibrated trace gas containing 73.2+/– 1.5 ppm of CO, acquisition time of 300 s. Right, 20.3+/– 0.4 ppm of SO_2, total acquisition time of 600 s.

Table 2
Experimentally determined trace detection limits using CEAS. Stated line strengths for pure gases [23]. Trace gasses supplied by Messer, either containing a single target species (HCN, H_2S) or multiple species in a single calibrated mixture*. Acquisition configuration, step 10 kHz, span 20 MHz, total acquisition time 600 s.

Species	Frequency (GHz)	Line strength (cm^{-1}/(molecule.cm^{-2}))	Trace concentration (ppm)	LOD (ppb)
SO_2	624.345	1.85×10^{-21}	20.3+/–0.4 *	140
CO	576.267	3.28×10^{-22}	73.2+/–1.5 *	700
NO	651.433	2.85×10^{-22}	41.1+/–0.8 *	1000
HCN	620.404	2.52×10^{-19}	0.64+/–0.02	1.2
H_2S	650.374	3.39×10^{-21}	53.1+/–1.1	110

the successive acquisitions, CO and baseline. The baseline is dominated by the numerous standing waves. They are caused by the unwanted reflections from the lenses, windows, and horn antennae. These variations are slower than the narrow molecular and can be removed by subtracting the measured baseline from the molecular spectrum. Alternatively, the baseline can be reliably predicted using the extremities of the spectra fitted with a suitable polynomial function as indicated by the red line in Fig. 5 left-hand. The SNR of the molecular signal observed is determined by evaluating the amplitude of the CEAS signal compared to the baseline noise. The signal is the difference between the CEAS signal and the baseline at the line centre. The baseline noise is evaluated away from the line centre and represents the small random variations that do not originate from the standing waves. These parameters are visually indicated in Fig. 5 left-hand pane, the noise is similar to the line thickness but is calculated by using a standard deviation. The CO spectrum displays an SNR of 102 leading to a Limit of Detection (LOD) of 720 ppb for this molecule, the LOD corresponds to the first observable detection (SNR=1). The right-hand pane of Fig. 5 shows a transition of SO_2 for a concentration of 20.3 ppm. This molecule has a stronger line strength, tabulated at 1.85×10^{-21} cm^{-1}/(molecule.cm^{-2}) for a pure gas [23], leading to an LOD of 140 ppb. Several calibrated trace gases have been assessed in this manner and the LOD values are presented in Table 2. The same information can be used to estimate the weakest observable line strength for a pure gas, here indicating a limit of 3×10^{-28} cm^{-1}/(molecule.cm^{-2}).

4.2. Cavity Ring-Down Spectroscopy (CRDS)

The principal shortcoming of the CEAS signal is that it is not directly quantitative. Trace detection undertaken relies on the measurement of a known standard sample under the same conditions. An alternative to the CEAS is to measure the photon residency time in the cavity and examine its variation with the presence of a gas. This technique developed in the infrared is therefore known as Cavity Ring-Down Spectroscopy [24]. One challenge of CRDS in the infrared is to match the laser frequency to

the cavity. In the case of the THz the AMC is much more frequency stable and is more readily matched to the cavity operating at longer wavelengths. The available source power and detector sensitivities are however more challenging for THz frequencies. To measure the cavity ring-down time τ the AMC must be coupled to the cavity to allow the intra-cavity power to build up. Once a stable power level is obtained the source must be rapidly removed and the acquisition triggered. The light exiting the cavity is measured with time and generally averaged for a large number of ring-down events. In our case the cavity is locked to the AMC frequency in the same way as for CEAS. A pulse modulation or AM is used to rapidly remove the source power and provides 50×10^3 events per second. The signal from the detector is amplified then measured by a dedicated data acquisition card (Spectrum Instruments) that samples at 1.25 GS/s and calculates the average waveform in real time, Fig. 6. Two different AMC sources have been used with this configuration, the first specified to provide –21 dBm as used in the previous sections. This has been compared to a more powerful source able to produce 0 dBm (Lytid). The disadvantage of this source is that it covers a much smaller frequency range.

The left-hand pane of Fig. 7 shows the SO_2 transition measured for an industrial sample extracted prior to the scrubber of the energy recovery facility in Dunkerque, France [25]. The cavity ring-down time is measured as a function of frequency, inset Fig. 7. The absorption coefficient α is determined [24] using the values with and without the sample gas being present. The absorption profile is fitted with a Voigt function for a pressure of 0.38 mbar to account for the Doppler and collisional broadening contributions. The SO_2 concentration is quantified by the integrated line area and calculated using the tabulated line strength of 1.85×10^{-21} cm^{-1}/(molecule.cm^{-2}) [23] to obtain 87+/–13 ppm. The pressure inside the cavity is determined using the collisional linewidth and the air broadening coefficient. The uncertainty of the concentration is dominated by that of the line strength at 5 % and the air broadening coefficient 10 %. The line can be observed at weaker concentrations than this uncertainty, as described by the LOD which is 300 ppb in this case. The same sample was also independently measured using a certified portable gas analyser (HORIBA PG-350EU) that employs a non-dispersive infrared technique for SO_2 giving 82+/– 2 ppm in good agreement with our quantification. The LOD was determined for the CRDS configuration by measuring the spectra for the calibrated trace gases used in the previous section, this was also performed for the High Power (HP) source at the available frequencies, Table 3. All of the species with lines strengths greater that 10^{-21} cm^{-1}/(molecule.cm^{-2}) can be detected at sub ppm levels.

A particularly weak absorption was sought in order to assess the smallest variation on the absorption coefficient that can be observed with the HP AMC. A minority isotope $^{18}O^{13}C^{34}S$ of carbonyl sulphide was selected with a natural abundance of 0.94×10^{-6}. The line strength of this isotope is not directly tabulated, however its peak absorption coefficient has already been determined $\alpha_{OCS} = 4.3 \times 10^{-8}$ cm^{-1} at 587.116 GHz [26]. The CRDS measurement, Fig. 7 right-hand pane, shows peak a variation of 2.5 ns of the ring-down time, which corresponds to $\alpha = 5 \times 10^{-8}$ cm^{-1}, in agreement with the published value. We therefore estimate the minimum detectable absorption coefficient to be $\alpha_{\min} = 2 \times 10^{-8}$ cm^{-1} for these conditions.

4.3. Atmospheric losses

In addition to making sensitive high-resolution THz spectroscopy this instrument is able to quantify the total cavity losses. It can be used to accurately quantify the propagation losses caused by the atmosphere. This can be undertaken measuring the linewidth of any cavity mode. All of the 193 modes in the band 570 to 630 GHz were rapidly scanned in AM, with no cavity locking. The recorded profile of each mode is fitted using a Lorentzian function to extract the line width and determine the finesse F. The procedure is followed for an empty cell and after allowing a given pressure of the laboratory air into the cavity. Provided that the cavity losses $C_L = 1 - R.e^{-\alpha L}$ are small, then they are given by $C_L = \pi/F$. The atmospheric propagation losses per unit distance A_L are then,

$$A_L = \frac{\pi}{L}\left(\frac{1}{F_{air}} - \frac{1}{F_0}\right)$$

where F_{air} and F_0 are the measured values of finesse with the air sample and for an empty cavity respectively. The atmospheric losses were measured for the laboratory air for pressures from 200 to 1000 mbar, Fig. 8. In this band there is a strong influence originating from the absorption by water vapor. The laboratory air was at 22.5 °C with a relative humidity ranging from 48 to 53 % during these measurements. The water line at 620.700 GHz has a line strength of 5.67×10^{-21} cm^{-1}/(molecule.cm^{-2}) [23] clearly increases in surface area as the pressure is increased due to the pressure broadening. Although its line centre is outside of the measurement range the water line at 556.936 GHz, with a line strength of 5.2×10^{-20} cm^{-1}/(molecule.cm^{-2}), [23] has a very strong effect below 600 GHz and particularly at the higher pressures. The measured values are smaller than those reported elsewhere [27], for example the peak absorption for a relative humidity of 50 % at atmospheric pressure was 0.09 m^{-1}, whereas our measurements gave 0.05 m^{-1}. This may be due to the adsorption of a fraction of the water molecules onto the metallic cell wall. The total cavity losses under vacuum conditions and for 200 mbar are shown in the inset of Fig. 8. Even under vacuum the influence of some residual

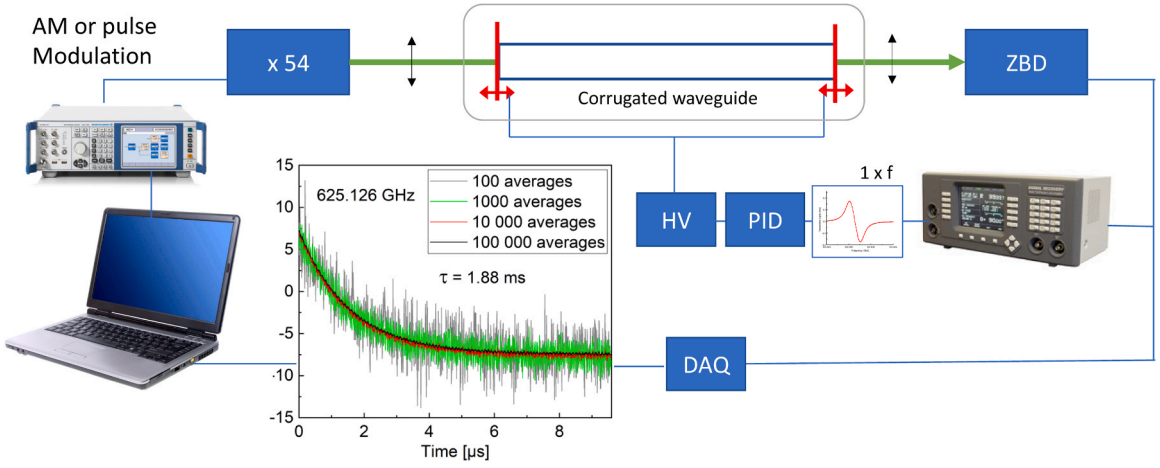

Fig. 6. CRDS configuration. Data acquisition is triggered at the end of the source pulse. Typical average ring-down signal are shown for acquisition lengths varying from 100 to 10^5 waveforms.

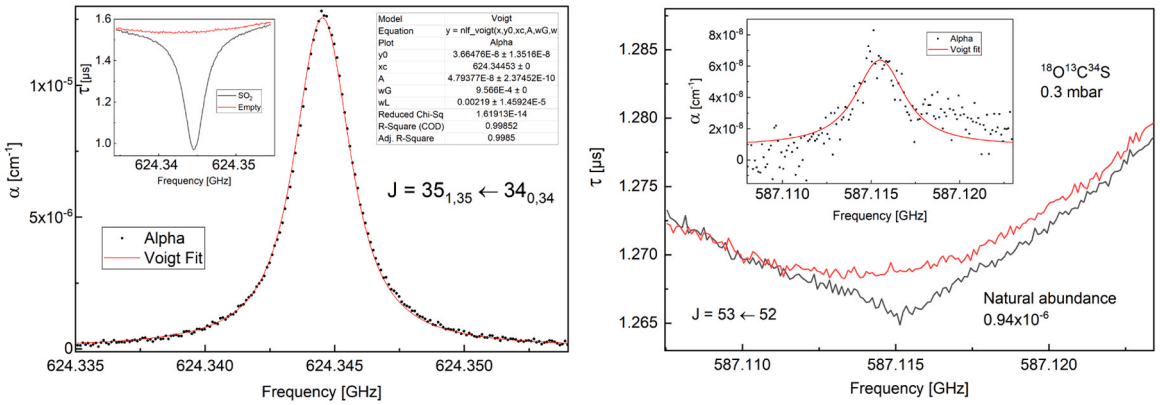

Fig. 7. Example spectra of CRDS. Left, SO_2 transition observed in an industrial gas sample at 0.38 mbar, 5×10^4 ring-down events per measurement point, step size 100 kHz, total acquisition time of approximately 200 s. Right, weak absorption of $^{18}O^{13}C^{34}S$ measured with 10^5 ring-down events per point, step size 100 kHz, total acquisition time of 300 s.

Table 3
Cavity Ring-Down Spectroscopy detection limits LOD for the standard AMC source, and LOD HP for high power AMC. Stated line strengths for pure gases [23]. Acquisition configuration, 10^5 ring-down events per point, step size 100 kHz, span 20 MHz, total acquisition time of 400 s.

Species	Frequency (GHz)	Line strength (cm^{-1}/(molecule.cm^{-2}))	LOD (ppb)	LOD HP (ppb)
SO_2	586.556	1.43×10^{-21}	400	70
SO_2	589.271	1.88×10^{-21}	400	60
SO_2	624.345	1.85×10^{-21}	300	
CO	576.267	3.28×10^{-22}	3000	130
NO	651.433	2.85×10^{-22}	1300	
NO	567.078	4.12×10^{-23}	13,000	1500
H_2S	579.799	2.16×10^{-21}	300	30
H_2S	650.374	3.39×10^{-21}	170	
HCN	620.404	2.52×10^{-19}	2	

moisture is observed, nevertheless a small increase in the losses is clearly visible at 200 mbar. We therefore estimate the minimum observable variation to be in the order of 0.001 m^{-1}.

5. Conclusion

The combination of an oversized corrugated waveguide and a pair of homemade Bragg mirrors have enabled the construction of a high-finesse THz cavity. The performance of these components is critical to minimise the cavity losses, finesse values of around 4000 have allowed interaction lengths of around 1.2 km to be achieved with this tabletop setup containing a gas cell with a physical length of 50 cm. Evaluation of the spectrometer's sensitivity has shown that pure gas with line strengths as weak as 3×10^{-28} cm^{-1}/(molecule.cm^{-2}) may be observed. The measurement of the photon residency time, or ring-down time gives direct access to a quantitative absorption coefficient. The minimum observable variation has been experimentally assessed using a triple isotope of OCS and is established at $\alpha_{min} = 2 \times 10^{-8}$ cm^{-1}. When applied to the trace gas concentration this limit typically translates to sub ppm detection levels. A simple AM configuration without a control loop has been used to determine the atmospheric propagation losses from 570 to 630 GHz. Further increases to the instrument sensitivity using this approach will require a reduction in the losses of both the mirrors and waveguide. Extending this approach to higher frequencies is presently limited by the fabrication of the waveguide requiring smaller corrugation dimensions.

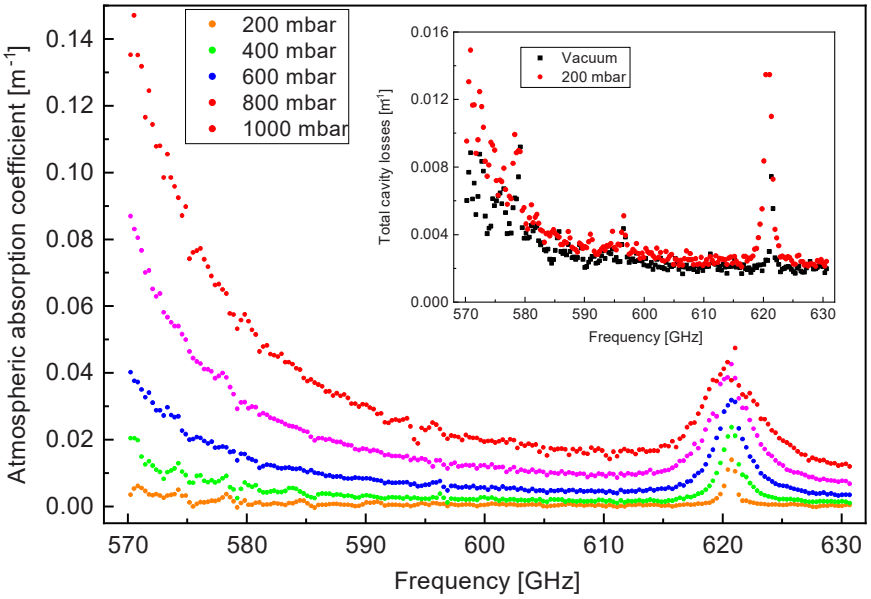

Fig. 8. Atmospheric losses measured using the cavity finesse for laboratory air at 22.5 °C, relative humidity from 48 to 53 %.

CRediT authorship contribution statement

Ducournau Guillaume: Resources. **Fourmentin Marc:** Software. **Cuisset Arnaud:** Formal analysis, Methodology. **HINDLE Francis:** Conceptualization, Formal analysis, Methodology, Software, Validation, Writing – original draft, Writing – review & editing, Supervision. **Lampin Jean-François:** Investigation, Resources. **Mouret Gaël:** Formal analysis, Funding acquisition, Methodology, Project administration, Supervision, Validation, Conceptualization. **Elamleh Coralie:** Data curation, Investigation. **Decker Jean:** Resources. **Simon Fabien:** Data curation, Investigation, Writing – original draft.

Declaration of Competing Interest

The authors declare the following financial interests/personal relationships which may be considered as potential competing interests Gael Mouret reports financial support was provided by SATT Nord. Gael Mouret reports financial support was provided by French National Research Agency. Gael Mouret has patent ##WO/2019/002139 issued to SATT Nord. If there are other authors, they declare that they have no known competing financial interests or personal relationships that could have appeared to influence the work reported in this paper.

Data Availability

Data will be made available on request.

Acknowledgements

The authors would like to acknowledge the financial support of SATT Nord, the TERAWASTE project (CPER IRenE, phase 5), the French Agence Nationale de la Recherche via projects TIGER (ANR-21-CE30-0048) and WASPE (ANR-22-CE42-0024). This work was carried out within the framework of the Contrat de Plan État-Region (CPER) WaveTech@HdF, which is supported by the Ministry of Higher Education and Research, the Hauts-de-France (HdF) Regional Council, the Lille European Metropolis (MEL), the Institute of Physics of the French National Centre for Scientific Research (CNRS) and the European Regional Development Fund (ERDF).

References

[1] T. Amini, F. Jahangiri, Z. Ameri, M.A. Hemmatian, A review of feasible applications of THz waves in medical diagnostics and treatments: feasible applications of THz waves in medicine, J. Lasers Med. Sci. 12 (2021) e92-e92.
[2] L. Yu, et al., The medical application of terahertz technology in non-invasive detection of cells and tissues: opportunities and challenges, RSC Adv. 9 (17) (2019) 9354–9363, https://doi.org/10.1039/C8RA10605C.
[3] J.F. Federici, et al., THz imaging and sensing for security applications—explosives, weapons and drugs, Semicond. Sci. Technol. 20 (7) (2005) S266, https://doi.org/10.1088/0268-1242/20/7/018.
[4] P. Hlosta, M. Nita, D. Powala, W. Świderski, Terahertz radiation in non-destructive testing of composite pyrotechnic materials, Compos. Struct. 279 (2022) 114770, https://doi.org/10.1016/j.compstruct.2021.114770.
[5] T. Nagatsuma, K. Oogimoto, Y. Inubushi, J. Hirokawa, Practical considerations of terahertz communications for short distance applications, Nano Commun. Netw. 10 (2016) 1–12, https://doi.org/10.1016/j.nancom.2016.07.005.
[6] T. Nagatsuma, G. Ducournau, C.C. Renaud, Advances in terahertz communications accelerated by photonics, Art. no. 6, Nat. Photon 10 (6) (2016), https://doi.org/10.1038/nphoton.2016.65.
[7] F. Hindle, et al., Monitoring of food spoilage by high resolution THz analysis, Analyst 143 (22) (2018) 5536–5544, https://doi.org/10.1039/C8AN01180J.
[8] C. Kulesa, Terahertz spectroscopy for astronomy: from comets to cosmology', IEEE Trans. Terahertz Sci. Technol. 1 (1) (2011) 232–240, https://doi.org/10.1109/TTHZ.2011.2159648.
[9] M. Harwit, The Herschel mission, Adv. Space Res. 34 (3) (2004) 568–572, https://doi.org/10.1016/j.asr.2003.03.026.
[10] S. Heyminck, U.U. Graf, R. Güsten, J. Stutzki, H.W. Hübers, P. Hartogh, GREAT: the SOFIA high-frequency heterodyne instrument, A&A 542 (2012) L1, https://doi.org/10.1051/0004-6361/201218811.
[11] P. Cortes et al., 'ALMA Cycle 10 Technical Handbook', Apr. 2023, doi: 10.5281/ZENODO.4511521.
[12] J.W. Waters, et al., The Earth observing system microwave limb sounder (EOS MLS) on the aura Satellite', IEEE Trans. Geosci. Remote Sens. 44 (5) (2006) 1075–1092, https://doi.org/10.1109/TGRS.2006.873771.
[13] W. Wang, Z. Wang, Y. Duan, Performance evaluation of THz atmospheric limb sounder (TALIS) of China, Atmos. Meas. Tech. 13 (1) (2020) 13–38, https://doi.org/10.5194/amt-13-13-2020.
[14] S. Kassi, A. Campargue, Cavity ring down spectroscopy with 5 × 10−13 cm−1 sensitivity, J. Chem. Phys. 137 (23) (2012) 234201, https://doi.org/10.1063/1.4769974.
[15] V.L. Bratman, et al., High-gain wide-band gyrotron traveling wave amplifier with a helically corrugated waveguide, Phys. Rev. Lett. 84 (12) (2000) 2746–2749, https://doi.org/10.1103/PhysRevLett.84.2746.
[16] E.J. Kowalski, et al., Linearly polarized modes of a corrugated metallic waveguide, IEEE Trans. Microw. Theory Tech. 58 (11) (2010) 2772–2780, https://doi.org/10.1109/TMTT.2010.2078972.
[17] E.A. Nanni, S.K. Jawla, M.A. Shapiro, P.P. Woskov, R.J. Temkin, Low-loss transmission lines for high-power Terahertz radiation, J. Infrared Millim. Terahertz Waves 33 (7) (2012) 695–714, https://doi.org/10.1007/s10762-012-9870-5.
[18] F. Hindle, R. Bocquet, A. Pienkina, A. Cuisset, G. Mouret, Terahertz gas phase spectroscopy using a high-finesse Fabry–Pérot cavity, Optica 6 (12) (2019) 1449, https://doi.org/10.1364/OPTICA.6.001449.
[19] T. Chen, P. Liu, J. Liu, Z. Hong, A terahertz photonic crystal cavity with high Q-factors, Appl. Phys. B 115 (1) (2014) 105–109, https://doi.org/10.1007/s00340-013-5579-y.
[20] W. Withayachumnankul, B.M. Fischer, D. Abbott, Quarter-wavelength multilayer interference filter for terahertz waves, Opt. Commun. 281 (9) (2008) 2374–2379, https://doi.org/10.1016/j.optcom.2007.12.094.
[21] K. Ohkubo, S. Kubo, H. Idei, M. Sato, T. Shimozuma, Y. Takita, Coupling of tilting Gaussian beam with hybrid mode in the corrugated waveguide, Int. J. Infrared Milli Waves 18 (1) (1997) 23–41, https://doi.org/10.1007/BF02677895.
[22] D. Romanini, I. Ventrillard, G. Méjean, J. Morville, E. Kerstel, Introduction to cavity enhanced absorption spectroscopy (in Springer Series in Optical Sciences), in: G. Gagliardi, H.-P. Loock (Eds.), Cavity-Enhanced Spectroscopy and Sensing, Springer, Berlin, Heidelberg, 2014, pp. 1–60, https://doi.org/10.1007/978-3-642-40003-2_1 (in Springer Series in Optical Sciences).
[23] I.E. Gordon, et al., The HITRAN2020 molecular spectroscopic database, J. Quant. Spectrosc. Radiat. Transf. 277 (2022), https://doi.org/10.1016/j.jqsrt.2021.107949.
[24] J.H. van Helden, R. Peverall, G.A.D. Ritchie, Cavity enhanced techniques using continuous wave lasers, Cavity Ring- Spectrosc.: Tech. Appl. (2010) 27–56, https://doi.org/10.1002/9781444308259.ch2.
[25] C. Elmaleh, et al., THz cavity ring-down quantitative gas phase spectroscopy, Talanta (2022) 124097, https://doi.org/10.1016/j.talanta.2022.124097.
[26] K. Kubo, T. Furuya, S. Saito, Submillimeter-wave spectrum of carbonyl sulfide: rare isotopic species, J. Mol. Spectrosc. 222 (2) (2003) 255–262, https://doi.org/10.1016/j.jms.2003.09.001.
[27] D.M. Slocum, E.J. Slingerland, R.H. Giles, T.M. Goyette, Atmospheric absorption of terahertz radiation and water vapor continuum effects, J. Quant. Spectrosc. Radiat. Transf. 127 (2013) 49–63, https://doi.org/10.1016/j.jqsrt.2013.04.022.